Surface & Coatings Technology 324 (2017) 57–63

Contents lists available at ScienceDirect

Surface & Coatings Technology

journal homepage: www.elsevier.com/locate/surfcoat

Cold spray deposition of an icosahedral-phase-strengthened aluminum alloy coating

T.J. Watson [a], A. Nardi [b], A.T. Ernst [c], I. Cernatescu [a], B.A. Bedard [c], M. Aindow [c,*]

[a] Pratt & Whitney, Materials & Process Engineering, Structural Alloys and Processes, 400 Main Street, Mail Stop 114-40, East Hartford, CT 06108, USA
[b] United Technologies Research Center, East Hartford, CT 06108, USA
[c] Department of Materials Science and Engineering, Institute of Materials Science, University of Connecticut, Unit 3136, 97 North Eagleville Road, Storrs, CT 06269-3136, USA

ARTICLE INFO

Article history:
Received 7 March 2017
Revised 4 May 2017
Accepted in revised form 18 May 2017
Available online 19 May 2017

Keywords:
Aluminum alloy
Cold spray
Composite microstructure
Quasicrystal

ABSTRACT

Preliminary cold spray trials have been performed using gas-atomized Al-Cr-Mn-Co-Zr alloy powder, which exhibits a nanocomposite structure with an Al matrix and 35 vol% of icosahedral quasicrystalline dispersoids. Consolidated material produced from this powder has been shown to exhibit a remarkable combination of mechanical properties and pitting corrosion resistance. The purpose of this research was to determine whether this nanocomposite material could form the basis of a hard, corrosion-resistant coating. The powder was screened and classified to a size range of 15–34 μm. Coatings of 180 μm in thickness were deposited using a He carrier gas with a gun temperature and pressure of 430 °C and 3.5 MPa, respectively. The coatings were hard (301 ± 25 HV), dense (<1% porosity), and adherent (no interfacial cracks or debonds). X-ray diffraction and electron microscopy data show that the nanocomposite powder microstructure is retained in the coating with no decomposition of the metastable quasicrystalline dispersoids to equilibrium crystalline phases. However, there were significant changes in the grain structure of the Al, both in the coating and in the underlying substrate. The grains are refined and equiaxed in the substrate, indicating that dynamic recovery/recrystallization occurs. Severely distorted flattened Al grains arise in the coating close (<1 μm) to the interface with the substrate, consistent with bonding via an adiabatic shear instability. The coating shows no pitting in 6-week salt fog exposures and seems to afford some protection to small exposed areas on adjacent bare substrate. These observations suggest that this material has very good potential to form the basis for a practical, hard, corrosion-resistant, quasicrystal-reinforced, nano-composite, cold-spray coating.

1. Introduction

Quasi-crystalline phases were first discovered in rapidly solidified Al-Mn alloys over 30 years ago [1–3], and these phases have now been found in a wide variety of ternary and higher order alloy systems. Quasicrystals exhibit a remarkable combination of properties including: high hardness, strength and elastic moduli; low surface energies and frictional coefficients; and good resistance to wear and corrosion [4–8]. While quasi-crystalline phases are generally too brittle to be considered for use in monolithic form, their properties do make them attractive as potential materials for wear-, oxidation- and/or corrosion-resistant coatings [9–12]. There are, however, significant challenges to be overcome when producing coatings from quasi-crystalline materials. The most common issues are cracking or delamination of the brittle coating, and very careful control of the deposition parameters is needed to avoid such effects [13–18]. An alternate approach is to incorporate a second, more ductile phase to form a composite coating that exhibits many of the attractive properties of the quasi-crystalline phase while reducing the probability of problems associated with its brittle behavior [19–23].

In our work, we have explored the use of powder metallurgy routes to produce aluminum metal-matrix composites with strengths and thermal stabilities that exceed those of conventional Al alloy systems. Initially, we studied Al - rare earth - transition metal alloy compositions on the margins of the glass-forming regime. By forming metastable glassy intermediates, we were able to bypass the solubility limits of FCC Al and thus obtain high volume fractions of intermetallic strengthening phases in the final devitrified material [24–28]. Our earlier attempts to extend this approach to Al/quasi-crystal composites were unsuccessful. A powder-processed Al-Mn-Ce alloy with a composition at which quasi-crystals had been formed in previous studies [29,30], gave instead a mixture of metastable crystalline phases including a previously unreported $Al_{20}Mn_2Ce$ compound [31]. Subsequent studies by Coury et al. [32,33] on melt-spun ribbons of various Al-Mn-Ce alloys have shown that the $Al_{20}Mn_2Ce$ compound is a common feature in these alloys, and that the compound may have been an unrecognized or mis-identified constituent in earlier work on this system [29,30].

* Corresponding author.
E-mail address: m.aindow@uconn.edu (M. Aindow).

http://dx.doi.org/10.1016/j.surfcoat.2017.05.049
0257-8972/

More recently, we have identified an Al-Cr-Mn-Co-Zr alloy for which nanocomposite powders can be produced by gas atomization [34]. These powders comprise a face-centered-cubic (FCC) Al matrix with ≈35% by volume of icosahedral phase (I-phase) quasi-crystalline dispersoids and a little Al_9Co_2. Bulk material was formed by warm blind-die compaction of canned powder, and it was shown that the I-phase dispersion was retained in the microstructure following consolidation. This bulk material exhibited a very attractive combination of room temperature mechanical properties including: a dynamic elastic modulus of 90.5 GPa, a tensile yield strength of 690 MPa, a tensile elongation to failure of 6%, and a high-cycle fatigue life of 10^9 cycles at an applied stress of 207 MPa with a stress ratio of $R = -1$. The composite retained a high tensile modulus (73 GPa) and yield strength (400 MPa) at a testing temperature of 300 °C, where most Al alloys would undergo catastrophic softening [34]. It was also found that this material has an extraordinary resistance to pitting corrosion. In salt fog exposures, the bulk material exhibited far lower corrosion pit densities and depths than commercial high-strength aerospace Al alloys tested under the same conditions [35]. Cross-sectional electron microscopy was used to reveal the structure of the oxide scale formed at the surface; from these data, it was inferred that the pitting corrosion resistance was due to the effects of Cr in the system, both in the Cr-rich I-phase and in the FCC Al solid solution. Thus, this material has excellent potential as the basis for high-strength, corrosion-resistant composite coatings. Here we report a preliminary study on the use of kinetic cold spray to produce coatings of this material using the nanocomposite gas-atomized powder as the feedstock in the spray process. It is shown that hard, dense, adherent coatings are produced, that the metastable I-phase is retained despite the adiabatic heating that occurs during particle/substrate impacts, and that these coatings exhibit a pitting corrosion resistance akin to that reported previously for the bulk consolidated material with this composition.

2. Materials and methods

The nano-composite powder used in these cold spray trials is the same as that used to produce the bulk material for our previous studies [34,35]. A master alloy with a composition of Al-2.6Cr-1.6Co-1.5Mn-0.5Zr (at.%) was produced at Great Western Technologies (Troy, Michigan) by vacuum induction melting and then casting into ingots. Powder was produced from this alloy at Valimet Company (Stockton, California) by melting in a crucible under Ar, performing gas atomization of the molten stream using high-pressure He gas, and then sieving to −450 mesh (≤34 μm). Before spraying, the powder was heated in air to 230 °C to drive off any adsorbed moisture, and then classified in N_2 gas to remove particles smaller than 15 μm. This latter process is necessary both to inhibit clumping during the powder feed and to avoid melting of the finer particles in the de Laval nozzle. The cold spray apparatus used in this study was a high pressure system designed and built at UTRC with a powder preheating/mixing chamber prior to the throat of the nozzle. For these experiments the preheating/mixing chamber length was 100 mm long, the throat diameter of the polybenzimidazole polymer nozzle was 1.72 mm, the throat to exit area ratio was 8.6, and the divergent section length was 150 mm. The powder was fed into the mixing chamber with a K-Tech powder feeder operating at 0.7 rpm and using N_2 carrier gas with a flow rate of 192 slpm. The gun temperature was maintained at 430 °C, and the main spray gas was He flowing at 1596 slpm, giving a gun pressure of 3.5 MPa. Under these conditions, the cold N_2 carrier gas does not dilute the main He spray gas substantially. While velocity measurements were not performed for these spray trials, the mean particle velocity was estimated using a model which predicts velocities based upon the process conditions, nozzle geometry and material properties. This model has been calibrated to laser Doppler velocimeter data obtained using this nozzle geometry and material using Al 5056 alloy powder with a similar size range. For a 20 μm particle sprayed under the conditions used here, the calculated velocity was 1462 m/s. Deposition was performed onto sheet substrates of A1 6061 in the T6 condition. Immediately prior to depositing the coatings, the substrate surfaces were prepared by abrading with silicon carbide paper, rinsing, and then wiping with solvent to eliminate surface moisture. The stand-off distance between the nozzle and the substrate was 32 mm, and the gun traverse rate was 200 mm/s.

The coating microstructures were evaluated using X-ray diffraction (XRD), visible light microscopy (VLM), scanning electron microscopy (SEM) and transmission electron microscopy (TEM). The XRD data were acquired in Bragg-Brentano geometry in a PANalytical Empyrean diffraction system with CuKα radiation. Data were acquired with a scan step of 0.016° over a 2θ range of 10–95°. For VLM and SEM studies, portions of the coated coupons were mounted in cross-section, then ground and polished using conventional metallographic techniques. For VLM these cross-sections were etched using Keller's reagent, whereas for SEM they were examined in the as-polished condition. Back scattered electron (BSE) SEM images were obtained using an FEI Teneo LoVac SEM operating in high vacuum mode at an accelerating voltage of 5 kV. For TEM studies, cross-sectional specimens were produced using a FEI Helios Nanolab 460F1 dual-beam FIB equipped with a flip-stage and a scanning TEM (STEM) detector. A 2 μm-thick Pt layer was deposited onto the area of interest using the ion beam. The accelerating voltage on the Ga + ion column was maintained at 30 kV, but to minimize ion beam damage or implantation, the ion beam current was gradually decreased during milling to a final value of 7.7 pA. The FIB-cut specimens were mounted onto Cu Omni grids and these were examined in a FEI Talos F200X S/TEM operating at an accelerating voltage of 200 kV.

Measurements of Vickers hardness were obtained from the metallographic cross-sections using a Leco LM248 micro-hardness tester with a 100 g load. The pitting corrosion resistance was evaluated by exposing coated coupons for times of up to 1008 h (six weeks) in a salt-fog chamber according to ASTM B117-09 [36]. The specific conditions used were: 35 °C, 95% humidity, 5 g/L NaCl, and a plate angle of 10° from the vertical. The exposed plates were cleaned following ASTM G1-03 [37], then the depths of the pits were evaluated using VLM. To test the possibility of galvanic effects between the coating and substrate, a rectangular coupon of A1 6061 with dimensions 40 × 120 mm was coated on one end, and shallow recesses of defined geometry were then milled through the coating to expose the underlying metal. These coupons were subjected to salt fog exposure under the same conditions for 1008 h, and the pits formed in the substrate were evaluated. Too few pits were observed for meaningful values of pit density to be obtained. Values of maximum pit depth were measured by identifying the largest pit in each square, and then taking the difference between the VLM objective lens heights when focusing on the top and bottom of the pit.

3. Results

The coatings produced in these preliminary trials were dense, adherent, and relatively uniform. Examples of VLM images from etched metallographic cross-sections are shown in Fig. 1. Low magnification images such as Fig. 1(a) show that the coating has a mean thickness of ≈180 μm, but that this varies locally from around 150 μm to 210 μm due to the roughness of the coating surface and to the undulating coating/substrate interface. Higher magnification VLM images such as Fig. 1(b) show that the interface is abrupt and appears to be crack-free. Such images also suggest that the undulating interface morphology may correspond to the flow of the softer substrate material around the hard particle impacts at the start of the cold-spray process. We note that micro-hardness measurements taken from the coating in polished but un-etched metallographic cross-sections gave values of 301 ± 25 HV, whereas the bulk material produced from this alloy powder by blind-die compaction [34] has a hardness of 199 ± 2 HV, and a typical value for Al 6061 in the T6 condition is 107 HV [38].

The compositional uniformity of the coating was evaluated using BSE SEM images on polished cross-sections. Examples of such images

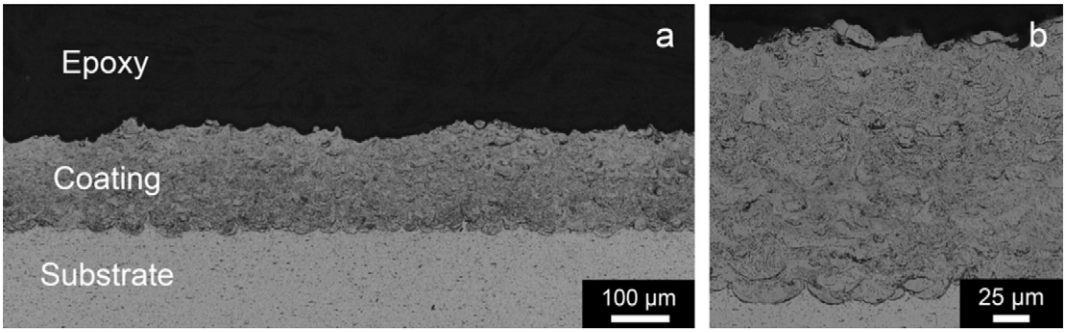

Fig. 1. VLM images from an etched metallographic section through a coated coupon: (a) low magnification overview; (b) detail showing the coating structure and interface morphology.

are shown in Fig. 2. The low magnification image in Fig. 2(a) covers the full coating thickness. In this image, the substrate appears dark because it comprises mainly FCC Al with up to 1.5% by volume of Mg_2Si and $(Fe,Mn)_3SiAl_{12}$ (e.g. [39].). The latter particles appear bright due to the higher backscattering cross-sections for Fe and Mn. Similarly, the coating appears brighter due to the Cr, Co, Mn and Zr in the alloy feedstock. There is one large (≈25 μm across) dark feature in the center of the field of view, which corresponds to an isolated Al-rich particle. There are also a few brighter features that correspond to local concentrations of heavier elements. Otherwise, the contrast is very uniform on this scale, corresponding to a uniform composition, as one might expect for cold spray from a gas-atomized powder feed. At higher magnifications, however, it is clear that the coating exhibits a composite microstructure with a dispersion of bright equi-axed features in a dark matrix (Fig. 2(b)). This is consistent with our previous observations on bulk material produced by consolidation of the same alloy powder, which exhibited a microstructure consisting of equi-axed I-phase dispersoids in an FCC Al matrix [33]. Moreover, the scale and distribution of the bright features in Fig. 2(b) varies significantly from location to location within this area, and a similar variation was observed in all of the other areas examined at this scale. Here again, this is consistent with our previous observations that the sizes of the I-phase dispersoids vary from particle to particle in the powder [34].

One concern in the processing of this material is that the I-phase could decompose to the corresponding crystalline approximants or other intermetallic phases due to the gas pre-heat and/or adiabatic heating upon particle impact. To test this, the character of the dispersoids in the cold-sprayed coatings was evaluated using a combination of XRD and TEM. Examples of the XRD data obtained from the gas-atomized feedstock powder and the cold-sprayed coating are shown in Fig. 3. The data from the powder is consistent with this being a two-phase mixture of FCC Al and I-phase as expected. The data from the coating reveal the same peaks, albeit somewhat weaker and broader than those from the powder. Further confirmation was obtained by TEM of FIB-cut specimens from the center of the coating.

Fig. 4 is a bright-field (BF) TEM image of a region containing dispersoids ≈ 200 nm in diameter. The inset selected area diffraction pattern (SADP) was obtained from the dispersoid marked "X" in the center of the field of view. This SADP exhibits the characteristic 5-fold pattern expected for the [000001] zone axis of the I-phase [40,41]. Thus, the bright dispersoids observed in BSE SEM images such as Fig. 2(b) are indeed retained I-phase, rather than any crystalline phase(s).

Further details on the microstructure at the coating/substrate interface were obtained from FIB-cut cross-sections. An example of a secondary electron (SE) SEM image obtained from the face of a FIB cut is shown in Fig. 5. The topographic contrast normally associated with such SE images is not evident because the surface is highly planar, and instead there is a combination of more subtle contrast features that reveal changes in both orientation and composition. The FCC Al matrix is dark in such images whereas the I-phase dispersoids and the intermetallic compounds are brighter. In the A1 6061 substrate, these bright features are mainly equi-axed Mg_2Si precipitates up to 200 nm in diameter. However, in the coating they are I-phase dispersoids 250–500 nm in diameter with fine (<75 nm) Al_9Co_2 precipitates in the Al matrix surrounding the I-phase. Similar features were observed in other areas except that (as discussed earlier) the size of the I-phase dispersoids varied from area to area within the coating. There are also interesting differences in the FCC Al grains in images such as Fig. 5. The grains in the substrate immediately below the coating are roughly equi-axed with diameters of around 1 μm, which is far less than the starting grain size for the substrate (≈15 μm). The grains in the coating are also equi-axed, but these are up to 200 nm in diameter, i.e. they are much smaller than those in the substrate.

Examples of BF TEM images from a thin FIB-cut lamella of the interface region are shown in Fig. 6. Lower magnification images such as Fig. 6(a) show that the interface is abrupt, and that there are fine

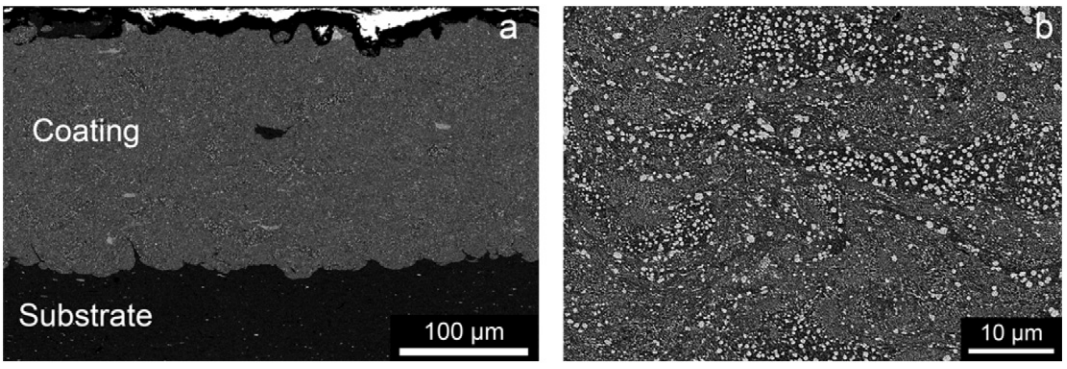

Fig. 2. BSE SEM images from the sample shown in Fig. 1 after re-polishing to remove the etched surface layer: (a) overview showing the uniformity of the coating, (b) detail showing the variation in the size and distribution of the dispersoids.

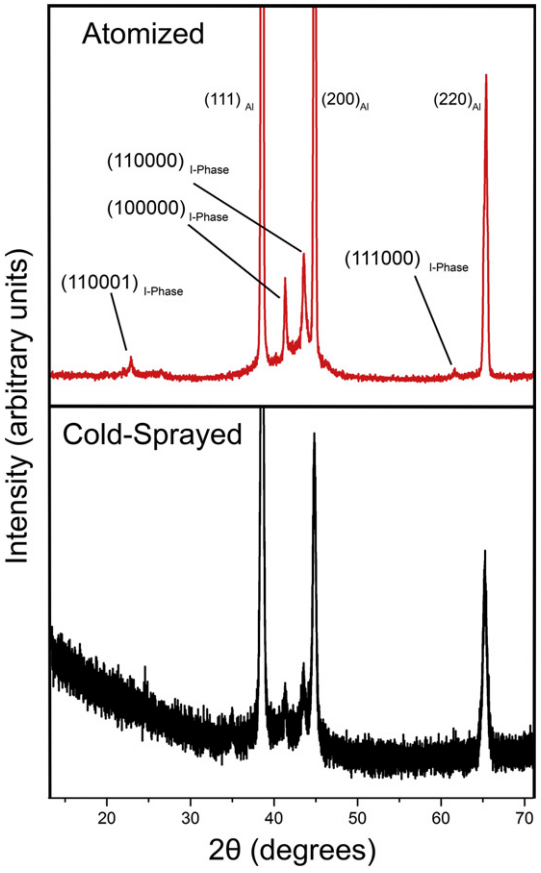

Fig. 3. XRD data obtained from: (a) the gas-atomized feedstock powder, (b) the cold-sprayed coating.

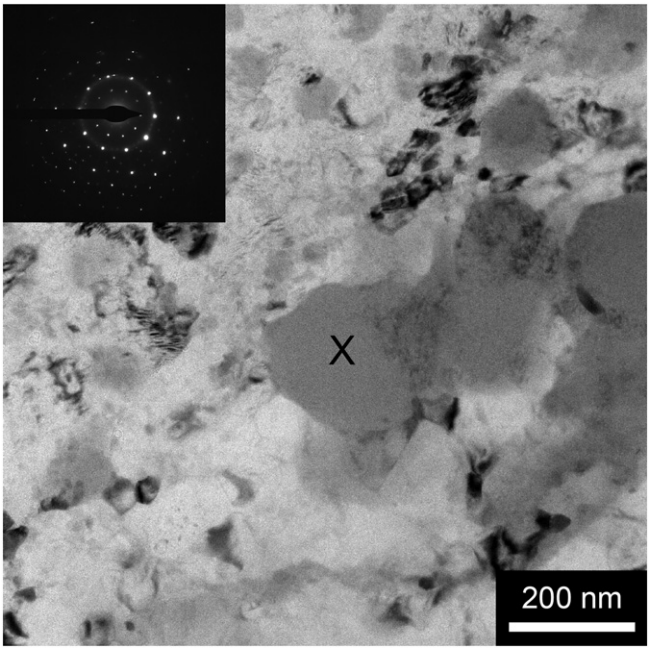

Fig. 4. BF TEM image from a FIB-cut specimen of the coating. The lighter regions around the outside are the Al grains, whereas the darker gray regions in the center and on the right are the I-phase dispersoids. The inset SADP is from the dispersoid marked X in the center of the image.

micro-cracks present in the coating parallel to the interface rather than between the coating and substrate. Both the coating and the substrate contain high densities of dislocations, although the dislocation density appears to be much higher in the coating. Higher magnification images such as Fig. 6(b) reveal that the most severely deformed region of the coating occurs in a band 1–2 μm thick at the interface. The grains within this band are flattened parallel to the interface and the thickness of these distorted grains is around 20 nm.

The coated samples that were subjected to salt fog exposures for up to 1008 h exhibited no detectable corrosion pits. Thus, the coatings appear to be even more resistant to pitting corrosion than the consolidated alloy formed from the same powder, since the consolidated material did form occasional pits when tested under the same conditions [35]. The part-coated coupon produced to evaluate possible galvanic effects between the coating and the substrate is shown in Fig. 7(a). The coated end is on the right in this figure, and the shallow (250 μm deep) recesses machined through the coating into the underlying alloy substrate are clearly visible. These recesses have two different geometries: slots 30 mm long and 0.4, 0.8 and 1.6 mm wide, and circles 1.6, 3.2, 6.4 and 12.8 mm in diameter. For comparison, circles of the same sizes were milled into the bare substrate on the left to cover the possibility that the machined surface might exhibit different pitting corrosion behavior than the original rolled and T6-tempered sheet. The exposed coupon and the surface after cleaning are shown in Figs. 7(b) and (c), respectively. The areas of the recesses are too small to obtain statistically significant measures of the pit densities, but we were able to obtain reproducible values of the maximum pit depth. The values are plotted in Fig. 8 as a function of the area of substrate metal exposed in each recess. These data appear to show a correlation between the area exposed and the maximum pit depth for both the circles and slots, with deeper pits being formed in the larger recesses.

4. Discussion

The kinetic cold spray technique is one of the most powerful and versatile approaches for producing coatings of metal matrix composites. This usually involves mixing separate powders of the metal matrix and reinforcement phases, and the combination of hard and soft particles seems to promote the formation of dense, adherent cold-spray coatings (e.g. [42]). A key advantage of using cold spray is that coatings of thermodynamically unstable phase mixtures and metastable phases can be formed; interfacial reactions and phase transformations are kinetically suppressed due to the limited heating from the carrier gas and from adiabatic effects. This approach has been applied successfully to produce hard, wear-resistant, metal/quasicrystal composite coatings from systems such as: tin-bronze/Al-Cu-Fe-B [20,22] and Ti/Al-Cr-Fe [23]. In both cases, dense coatings were produced with up to 20% by volume of the quasicrystalline reinforcement, but attempts to obtain even better properties by increasing this to 30% resulted in much higher porosity and poorer wear resistance [23]. Clearly, if one can produce in-situ composite particles by, for example, gas atomization then it might be possible to deposit dense coatings with higher volume fractions of the reinforcing phase because the parameters that control coating quality would be different. As far as we are aware, only two such systems have been studied: Al/Al-Cr-Fe-Ti-Co by Hishida et al. [43,44] and Al/Al-Fe-Cr(-Ti) by Kiz, Byakova, et al. [45,46]. In both cases, good bonding to the substrate and excellent mechanical properties were reported, but neither system appears to have been pursued beyond these initial reports.

Here we have considered the use of gas-atomized nanocomposite Al/Al-Cr-Mn-Co-Zr powder as the feedstock for cold-spray deposition of composite coatings. Our previous work on consolidated composite material produced from this powder showed that it exhibited an excellent combination of mechanical properties [34] and exceptional resistance to pitting corrosion [35]. It was thus our intention to perform preliminary trials to determine whether these properties could be

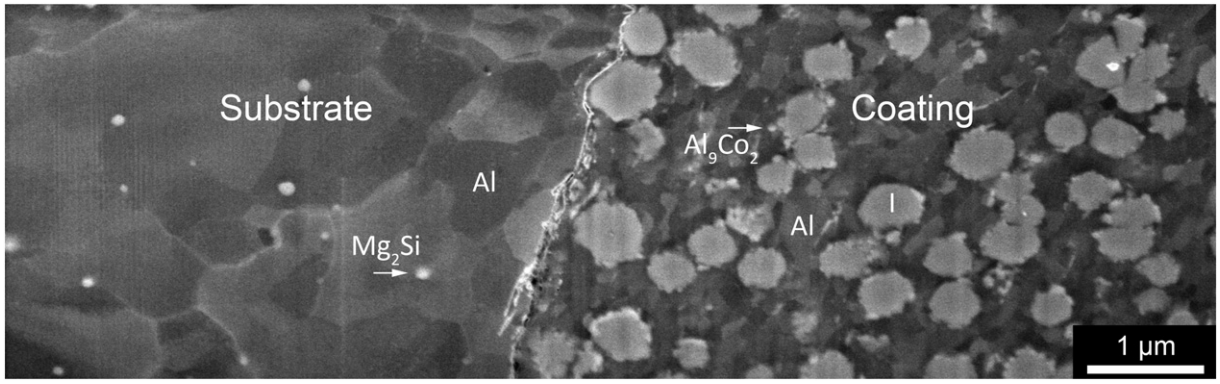

Fig. 5. SE SEM image from a FIB-cut section through the coating/substrate interface. The substrate comprises equiaxed Al grains with occasional Mg_2Si precipitates. The coating has an Al matrix with a much finer grain size, a high density of coarse I-phase dispersoids, and some very fine Al_9Co_2 precipitates.

exploited by using cold spray to produce wear and corrosion-resistant quasicrystal-reinforced nano-composite coatings.

Despite the use of default powder feed and spray conditions, rather than conditions optimized for this particular nanocomposite powder, very good quality coatings were obtained indicating that this type of material has excellent potential for use in the cold spray process. The coatings were dense (<1% porosity), fairly uniform, and appeared to adhere very well to the Al 6061 substrate. Cross-sections viewed using a range of microscopy techniques from VLM to TEM showed no evidence of de-bonding, spallation or any interfacial cracking. The undulating geometry of the coating/substrate interface suggests that in the initial stages of deposition the nanocomposite powder particles retain a near-spherical morphology, rather than the more typical flattened splat morphology exhibited by most metallic powders. This is consistent with the majority of the plastic strain being borne by the softer substrate during these initial impacts. Despite this partitioning of the strain, BF TEM images show that the defect density in the substrate is actually lower than that in the deposit. A possible explanation for this is suggested by the equiaxed morphology and the refined scale of the FCC Al grains in this region; this presumably develops due to dynamic recrystallization and/or recovery in the region immediately below the interface. Similar effects could be responsible for the refined equiaxed (albeit much finer) grains in the FCC Al matrix of the coating at distances of >1 μm from the interface. A combination of this grain refinement and the high dislocation density could account for the 50% higher hardness of the coating than that of the consolidated material produced from the same powder [34]. We note that there is a 1 μm thick unrecrystallized region in the deposit at the interface within which heavily distorted flattened grains lie parallel to the interface. This presumably corresponds to the zone of the adiabatic shear instability which is thought to lead to the development of strong bonds in most models for cold spray deposition (e.g. [47]).

It is important to note that while all quasi-crystalline phases are inherently meta-stable non-equilibrium forms, the XRD and TEM data obtained here show no evidence for the decomposition of the I-phase to the corresponding crystalline approximant phases, or indeed any other intermetallic phases. This is remarkable given the extent of the other microstructural changes that occur in the coating and the adjacent substrate, and the heating (both directly from the propellant gas and indirectly from adiabatic effects) that the powder particles must experience. In our previous study on consolidated material produced from this powder, we did find some evidence for the onset of such decomposition processes in samples forged at 300 °C. Since no such effects are observed here, we conclude that the I-phase is relatively stable under the conditions that prevail in cold spray deposition. This is perhaps because of the sluggish kinetics of the decomposition process so that there is insufficient time for such processes to occur during the short thermal transients that the powder particles experience during the cold spray process.

Next, we consider the pitting corrosion resistance of these coatings. It is truly remarkable that no pits were observed on any of the cold-sprayed samples even after 6 weeks of salt fog exposure. This leads us

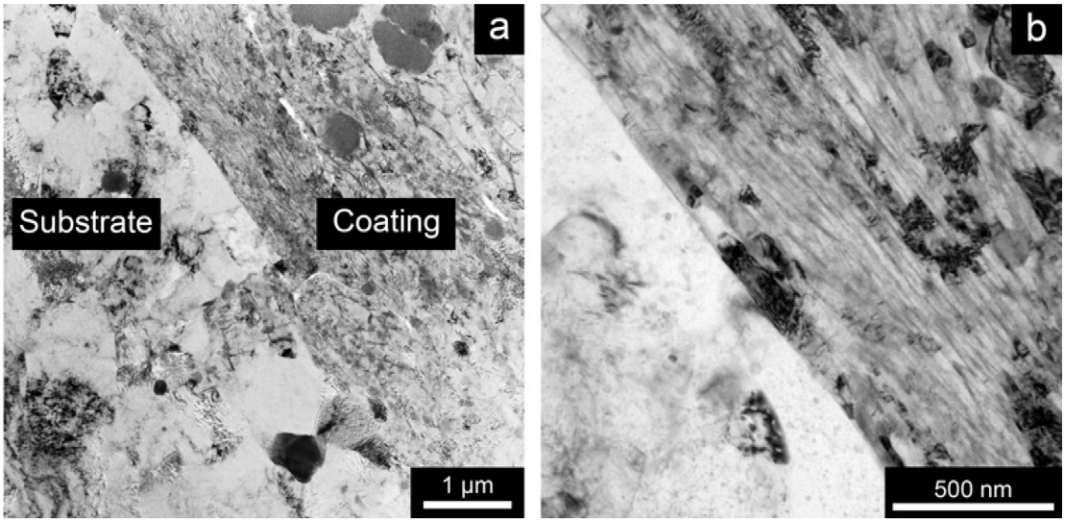

Fig. 6. BF TEM images from a FIB-cut specimen of the coating/substrate interface; the image in (a) is a detail of the region of the interface in the top left corner of (a).

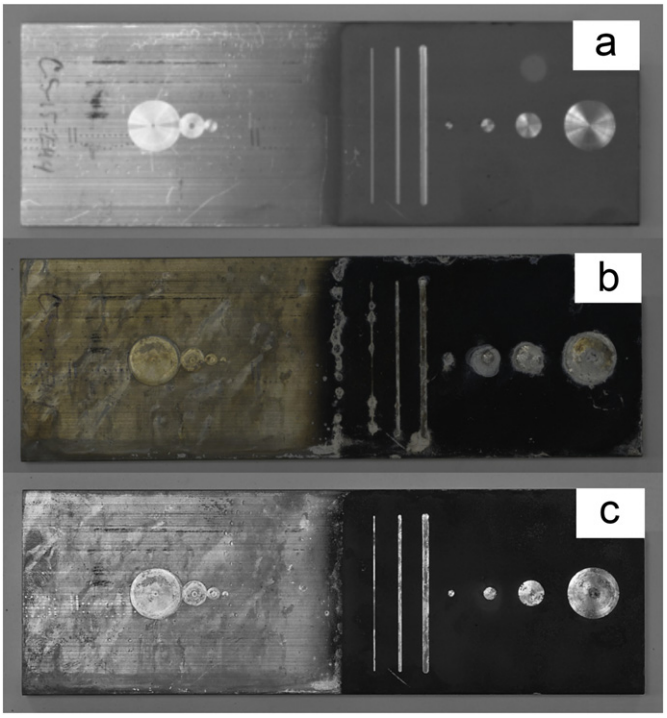

Fig. 7. Photographs of a partly-coated Al 6061 coupon 40 mm wide and 120 mm long, with circular holes and slots milled through the coating on the right and into the bare substrate on the left: a) before testing, b) after salt fog exposure, c) after cleaning for evaluation of pits.

to the surprising conclusion that the coating has an even higher resistance to pitting corrosion than the consolidated material produced using the same powder [35]. It was concluded previously that the pitting corrosion resistance in the consolidated material arises from the combined effects of the Cr-rich I-phase and Cr in solid solution in the FCC Al. Thus, there are two possible reasons for the enhanced pitting corrosion resistance of the cold-sprayed coatings. Firstly, the FCC Al matrix in the cold sprayed coating has a much higher density of defects (dislocations, grain boundaries, etc.) than the consolidated material. Such defects could act as short-circuit diffusion paths for species such as Cr to migrate to the surface and establish a thicker, more uniform

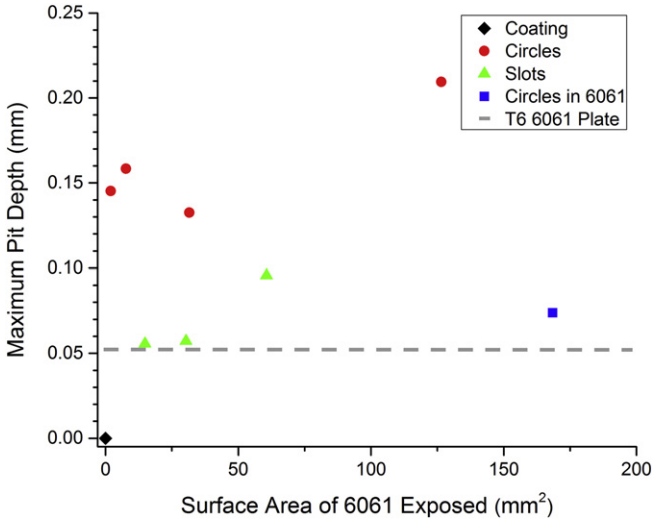

Fig. 8. Values of maximum pit depth as a function of exposed substrate area for the milled circles and slots in the sample shown in Fig. 7, and for the intact coating (0.0 because no pits are observed). The value for an uncoated T6 6061 plate sample exposed under the same conditions is shown as a horizontal dashed line for comparison.

passivating layer. Secondly, the porosity in the cold-sprayed coating is lower than that in the consolidated material. Since geometric pits are known to be potential sites for pitting corrosion in systems where the passivating film strongly inhibits pit nucleation, the difference could simply correspond to an absence of pre-existing pores on the coating surface.

The effect of the coating on the pitting corrosion behavior of adjacent exposed regions of the 6061 substrate is also interesting. The data in Fig. 8 show a correlation between the area exposed and the maximum pit depth, with deeper pits being formed in the larger recesses. We note that this is not a simple statistical sampling effect, with larger areas having a greater probability of containing a potent site for pit nucleation, because the maximum pit depths in the circular recesses milled through the coating are greater than those in the corresponding recesses in the adjacent bare substrate. Moreover, these values are all higher than those reported previously for bare A1 6061 in the T6 condition after being subjected to salt fog exposures using the same testing parameters [35]. The increase in pit depth with exposed area shows that this is not a simple galvanic effect. On the contrary, this trend indicates that exposed regions in close proximity to the coating may be afforded some limited protection from pitting, perhaps due to the diffusion of passivating Cr species from the adjacent coating. The formation of deeper pits in the circular recesses through the coating than in the slots for a given area exposed, lends further support to this hypothesis.

The data presented here are preliminary, and there is clearly much work to be done to develop a comprehensive understanding of the relationships between the nanocomposite powder chemistry and structure, the cold spray process variables, the microstructure of the resulting coatings, and their performance. Nonetheless, these initial observations do indicate that this material system has excellent potential to form the basis for practical wear and corrosion-resistant quasicrystal-reinforced nano-composite cold-spray coatings.

5. Conclusions

In this study it has been shown that nanocomposite powder produced from an Al-Cr-Mn-Co-Zr alloy by gas atomization can be used as the feedstock for cold spray deposition of quasi-crystal reinforced nanocomposite coatings onto Al6061 sheet substrates. The coatings produced here exhibit the same combination of phases as the feedstock powder, namely an FCC Al matrix with 35 vol% of icosahedral quasicrystalline dispersoids and a little Al_9Co_2. The coatings were hard, dense and adherent with no evidence of interfacial debonding. There is some refinement of the substrate grain structure just below the interface, and extensive distortion of the Al grain in the coating within 1–2 μm of the interface; these features are consistent with bonding via an adiabatic shear instability. The coatings also exhibit exceptional resistance to pitting corrosion in salt fog exposures, and there is no evidence for the formation of galvanic couples with adjacent exposed regions of substrate. Thus, this alloy could be the basis for the first practical quasi-crystal reinforced cold-spray coating with good wear properties and corrosion resistance.

Acknowledgements

This research was supported by Pratt & Whitney, FEI Corporation and the University of Connecticut Research Foundation. Portions of this work were performed using the facilities in the UConn/FEI Center for Advanced Microscopy and Materials Analysis (CAMMA).

References

[1] D. Shechtman, I. Blech, D. Gratias, J.W. Cahn, Metallic phase with long-range orientational order and no translational symmetry, Phys. Rev. Lett. 53 (1984) 1951–1953.
[2] D. Shechtman, I. Blech, The microstructure of rapidly solidified Al_6Mn, Metall. Trans. 16A (1985) 1005–1012.

[3] L. Bendersky, Quasicrystal with one-dimensional translational symmetry and a ten-fold rotation axis, Phys. Rev. Lett. 55 (1985) 1461–1463.
[4] K. Urban, M. Feuerbacher, M. Wollgarten, Mechanical behavior of quasicrystals, MRS Bull. 22 (1997) 65–68.
[5] Z.M. Stadnik (Ed.), Physical Properties of Quasicrystals, Springer, 1999.
[6] J.M. Dubois, P. Brunet, W. Costin, A. Merstallinger, Friction and fretting on quasicrystals under vacuum, J. Non-Cryst. Solids 334–335 (2004) 475–480.
[7] E. Huttunen-Saarivirta, Microstructure, fabrication and properties of quasicrystalline Al–Cu–Fe alloys: a review, J. Alloys Compd. 363 (2004) 150–174.
[8] J.M. Dubois, Properties and applications of quasicrystals and complex metallic alloys, Chem. Soc. Rev. 41 (2012) 6760–6777.
[9] J.M. Dubois, S.S. Kang, J. Von Stebut, Quasicrystalline low-friction coatings, J. Mater. Sci. Lett. 10 (1991) 537–541.
[10] J.M. Dubois, S.S. Kang, Y. Massiani, Application of quasicrystalline alloys to surface coating of soft metals, J. Non-Cryst. Solids 153–154 (1993) 443–445.
[11] J.E. Shield, J.A. Campbell, D.J. Sordelet, Mechanical properties of Al-Cu-Fe-based quasicrystalline coatings, J. Mater. Sci. Lett. 16 (1997) 2019–2021.
[12] M.F. Besser, T. Eisenhammer, Deposition and applications of quasicrystalline coatings, MRS Bull. 22 (1997) 59–64.
[13] S.S. Kang, J.M. Dubois, Tribological properties of quasicrystalline coatings, J. Mater. Res. 8 (1993) 2471–2481.
[14] E. Fleury, S.M. Lee, W.T. Kim, D.H. Kim, Effects of air plasma spraying parameters on the Al-Cu-Fe quasicrystalline coating layer, J. Non-Cryst. Solids 278 (2000) 194–204.
[15] E. Fleury, Y.-C. Kim, J.-S. Kim, H.-S. Ahn, S.-M. Lee, W.-T. Kim, D.-H. Kim, Sliding friction and wear behavior of Al-Ni-Co-Si quasicrystalline coatings deposited by the high-velocity oxy-fuel spraying technique, J. Mater. Res. 17 (2002) 492–501.
[16] S. Polishchuk, P. Boulet, A. Mézin, M.-C. de Weerd, S. Weber, J. Ledieu, J.-M. Dubois, V. Fournée, Residual stress in as-deposited Al–Cu–Fe–B quasicrystalline thin films, J. Mater. Res. 27 (2012) 837–844.
[17] Y. Fu, T. Peng, D. Yang, C. Sun, Y. Chen, Y. Gao, HVOF sprayed Al–Cu–Cr quasicrystalline coatings from coarse feedstock powders, Surf. Coat. Technol. 252 (2014) 29–34.
[18] S. Polishchuk, A. Ustinov, V. Telychko, A. Merstallinger, G. Mozdzen, T. Melnichenko, Fabrication of thick, crack-free quasicrystalline Al-Cu-Fe coatings by electron-beam deposition, Surf. Coat. Technol. 291 (2016) 406–412.
[19] D.J. Sordelet, M.F. Besser, J.L. Logsdon, Abrasive wear behavior of Al-Cu-Fe quasicrystalline composite coatings, Mater. Sci. Eng. A 255 (1998) 54–65.
[20] X. Guo, G. Zhang, W. Li, Y. Gao, H. Liao, C. Coddet, Investigation of the microstructure and tribological behavior of cold-sprayed tin-bronze-based composite coatings, Appl. Surf. Sci. 255 (2009) 3822–3828.
[21] B.N. Mordyuk, M.O. Iefimov, K.E. Grinkevych, A.V. Sameljuk, M.I. Danylenko, Structure and wear of Al surface layers reinforced with AlCuFe particles using ultrasonic impact peening: effect of different particle sizes, Surf. Coat. Technol. 205 (2011) 5278–5284.
[22] X. Guo, J. Chen, H. Yu, H. Liao, C. Coddet, A study on the microstructure and tribological behavior of cold-sprayed metal matrix composites reinforced by particulate quasicrystal, Surf. Coat. Technol. 268 (2015) 94–98.
[23] N.W. Khun, R.T. Li, K. Loke, K.A. Khor, Effects of Al-Cr-Fe quasicrystal content on tribological properties of cold-sprayed titanium composite coatings, Tribol. Trans. 58 (2015) 616–624.
[24] A.L. Vasiliev, M. Aindow, M.J. Blackburn, T.J. Watson, Phase stability and microstructure in devitrified Al-rich Al-Y-Ni alloys, Intermetallics 12 (2004) 349–362.
[25] N.J. Magdefrau, A.L. Vasiliev, M. Aindow, M.J. Blackburn, T.J. Watson, Effect of heat-treatment on the microstructure and hardness of a devitrified Al-3.0Y-3.0Gd-5.0Ni-1.0Fe-1.0Co alloy, Scr. Mater. 51 (2004) 485–489.
[26] A.L. Vasiliev, M. Aindow, M.J. Blackburn, T.J. Watson, The structure of ternary compounds in Al-Gd-Ni alloys, Intermetallics 13 (2005) 741–748.
[27] M.A. Gordillo, L.C. Zhang, T.J. Watson, M. Aindow, Effect of upset forging on microstructure and tensile properties in a devitrified Al-Y-Ni-Co alloy, J. Mater. Sci. 48 (2013) 3841–3851.
[28] M.A. Gordillo, B. Bedard, T.J. Watson, M. Aindow, Effect of heat-treatment on phase stability and grain coarsening in a powder-processed Al-Ni-Co-Zr-Y alloy, J. Mater. Sci. 49 (2014) 5866–5877.
[29] A. Inoue, M. Watanabe, H.M. Kimura, F. Takahashi, A. Nagata, T. Masumoto, High mechanical strength of quasicrystalline phase surrounded by fcc-Al phase in rapidly solidified Al-Mn-Ce alloys, Mater. Trans. JIM 33 (1992) 723–729.
[30] F. Schurack, J. Eckert, L. Schultz, Synthesis and mechanical properties of cast quasicrystal-reinforced Al-alloys, Acta Mater. 49 (2001) 1351–1361.
[31] M.A. Gordillo, I. Cernatescu, T.T. Aindow, T.J. Watson, M. Aindow, Phase stability in a powder-processed Al-Mn-Ce alloy, J. Mater. Sci. 49 (2014) 3742–3754.
[32] F.G. Coury, W.J. Botta, C. Bolfarini, C.S. Kiminami, M.J. Kaufman, Reassessment of the effects of Ce on quasicrystal formation and microstructural evolution in rapidly solidified Al–Mn alloys, Acta Mater. 98 (2015) 221–228.
[33] F.G. Coury, C.S. Kiminami, W.J. Botta, C. Bolfarini, M.J. Kaufman, Design and production of Al-Mn-Ce alloys with tailored properties, Mater. Des. 110 (2016) 436–448.
[34] T.J. Watson, M.A. Gordillo, I. Cernatescu, M. Aindow, Structure and mechanical properties in a powder-processed icosahedral-phase-strengthened aluminum alloy, Scr. Mater. 123 (2016) 51–54.
[35] T.J. Watson, M.A. Gordillo, A.T. Ernst, B.A. Bedard, M. Aindow, Salt fog corrosion behavior in a powder-processed icosahedral-phase-strengthened aluminum alloy, Corros. Sci. 121 (2017) 133–138.
[36] ASTM standard B117-09, Standard Practice for Operating Salt Spray (Fog) Apparatus, ASTM, West Conshohocken, PA, 2009.
[37] ASTM standard G1-03, Standard Practice for Preparing, Cleaning, and Evaluating Corrosion Test Specimens, ASTM, West Conshohocken, PA, 2011.
[38] SAE AMS 4027N, Aluminum Alloy, Sheet and Plate, 1.0Mg - 0.60Si - 0.28Cu - 0.20Cr (6061; -T6 Sheet, -T651 Plate), Solution and Precipitation Heat Treated, SAE International, Warrendale, PA, 2014.
[39] D. Maisonnette, M. Suery, D. Nelias, P. Chaudet, T. Epicier, Effects of heat treatments on the microstructure and mechanical properties of a 6061 aluminium alloy, Mater. Sci. Eng. A 528 (2011) 2718–2724.
[40] D. Levine, P.J. Steinhardt, Quasicrystals: a new class of ordered structures, Phys. Rev. Lett. 53 (1984) 2477–2480.
[41] V. Elser, Indexing problems in quasicrystalline diffraction, Phys. Rev. B 32 (1985) 4892–4898.
[42] A. Moridi, S.M. Hassani-Gangaraj, M. Guagliano, M. Dao, Cold spray coating: review of material systems and future perspectives, Surf. Eng. 36 (2014) 369–395.
[43] M. Hishida, M. Fujita, K. Sakaki, Fabrication of aluminum coating with dispersed nanoscale quasicrystalline particles by cold spray, J. Jpn. Inst. Metals 73 (2009) 421–428.
[44] M. Hishida, M. Fujita, K. Sakaki, Investigation of aluminum coating with dispersed nanoscale quasicrystalline particles produced by cold spray, in: B.R. Marple, M.M. Hyland, Y.-C. Lau, C.-J. Li, R.S. Lima, G. Montavon (Eds.),Expanding Thermal Spray Performance to New Markets and Applications: Proceedings of the International Thermal Spray Conference; Las Vegas, NV 2009, pp. 296–301.
[45] M.M. Kiz, A.V. Byakova, A.I. Sirko, Yu.V. Milman, M.S. Yakovleva, Cold spray coatings of Al-Fe-Cr alloy reinforced by nano-sized quasicrystalline particles, Ukr. J. Phys. 54 (2009) 594–599.
[46] A.V. Byakova, M.M. Kiz, A.I. Sirko, M.S. Yakovleva, Yu.V. Milman, Cold-sprayed coatings based on high strength aluminium alloys reinforced by quasicrystalline particles: microstructure and key properties, High Temp. Mater. Processes 29 (2010) 325–337.
[47] M. Grujicic, C.L. Zhao, W.S. DeRosset, D. Helfritch, Adiabatic shear instability based mechanism for particles/substrate bonding in the cold-gas dynamic-spray process, Mater. Des. 25 (2004) 681–688.